

# LatentSync: Audio Conditioned Latent Diffusion Models for Lip Sync

Chunyu Li<sup>1,2</sup> Chao Zhang<sup>1</sup> Weikai Xu<sup>1</sup> Jinghui Xie<sup>1,†</sup> Weiguo Feng<sup>1</sup>  
 Bingyue Peng<sup>1</sup> Weiwei Xing<sup>2,†</sup>  
<sup>1</sup>ByteDance <sup>2</sup>Beijing Jiaotong University

## Abstract

We present *LatentSync*, an end-to-end lip sync framework based on audio conditioned latent diffusion models without any intermediate motion representation, diverging from previous diffusion-based lip sync methods based on pixel space diffusion or two-stage generation. Our framework can leverage the powerful capabilities of *Stable Diffusion* to directly model complex audio-visual correlations. Additionally, we found that the diffusion-based lip sync methods exhibit inferior temporal consistency due to the inconsistency in the diffusion process across different frames. We propose *Temporal REpresentation Alignment (TREPA)* to enhance temporal consistency while preserving lip-sync accuracy. *TREPA* uses temporal representations extracted by large-scale self-supervised video models to align the generated frames with the ground truth frames. Furthermore, we observe the commonly encountered *SyncNet* convergence issue and conduct comprehensive empirical studies, identifying key factors affecting *SyncNet* convergence in terms of model architecture, training hyperparameters, and data preprocessing methods. We significantly improve the accuracy of *SyncNet* from 91% to 94% on the *HDTF* test set. Since we did not change the overall training framework of *SyncNet*, our experience can also be applied to other lip sync and audio-driven portrait animation methods that utilize *SyncNet*. Based on the above innovations, our method outperforms state-of-the-art lip sync methods across various metrics on the *HDTF* and *VoxCeleb2* datasets. Code and models are publicly available at <https://github.com/bytedance/LatentSync>.

## 1. Introduction

The task of lip sync involves the generation of accurate lip movements in a talking video based on corresponding speech, while maintaining the head pose and personal identity. This technique has broad applications in numerous practical domains, such as dubbing, virtual avatars, and

<sup>†</sup>Corresponding authors

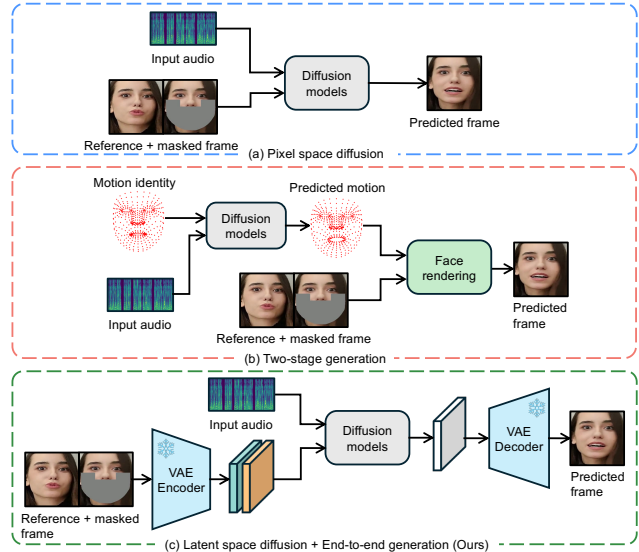


Figure 1. Frameworks comparison between previous diffusion-based lip sync methods and our method.

video conferencing.

In the field of lip sync, GAN-based methods [18, 36] remain the mainstream approaches. The main issue with GAN-based methods is that they struggle to scale up [24, 44] to large and diverse datasets due to the unstable training and mode collapse [6, 47]. Recent studies proposed diffusion-based methods [2, 29, 34, 57, 64] for lip sync, allowing the model to easily generalize across different individuals without the need for further fine-tuning on specific identities. However, these methods still have some limitations. Specifically, [2, 34] performs the diffusion process in the pixel space (Fig. 1 a), which restricts its ability to generate high-resolution videos due to the prohibitive hardware requirements. Methods like [57, 64] adopt a two-stage approach: the first stage generates lip motions from audio, and the second stage synthesizes the visual appearance conditioned on the motion (Fig. 1 b). The issue with this two-stage approach is that subtly different sounds may map to the same motion representation, which can result in the loss of nuanced expressions linked to the emotional tone of the

speech.

To solve the above problems, we propose LatentSync, a novel end-to-end lipsync framework based on audio conditioned latent diffusion models [41], without the need of any intermediate 3D representation [3] or 2D landmarks [5, 30], as shown in Fig. 1 (c). LatentSync leverages the powerful generative capabilities of Stable Diffusion [41] to directly capture the intricate audio-visual correlations, facilitating the generation of dynamic and lifelike talking videos.

Furthermore, we found that the lip-sync accuracy of our model was quite low without SyncNet [9, 36] supervision. We explored two methods to add SyncNet supervision to latent diffusion models [41]: (a) adding SyncNet supervision after decoding to pixel space, and (b) training a SyncNet in the latent space. However, we discovered that SyncNet has convergence issues in both high-resolution pixel space and latent space. To solve this problem, we conducted comprehensive empirical studies in the aspects of model architecture, training hyperparameters, and data preprocessing methods, allowing the SyncNet to converge easily. We achieved the unprecedented 94% accuracy on HDTF [62].

Additionally, we found that in comparison to single-step lip sync methods [18, 34, 36, 61], diffusion-based lip sync approaches [2, 34], which employ multi-step generation processes, exhibit inferior temporal consistency. We hypothesize that this might be due to the inconsistency in the diffusion process across different frames. Inspired by [15, 58], we proposed a new method called TREPA, which uses a large-scale self-supervised video model VideoMAE-v2 [52] to extract a powerful representation rich in temporal information. The distance between the temporal representations of the generated consecutive frames and the ground truth consecutive frames is used as an extra loss. This method is very similar to LPIPS [59], with the key difference being that this loss leverages temporal representations. We found that this simple method effectively improves the temporal consistency while preserving the lip-sync accuracy of our model.

In summary, we make the following contributions: (1) We proposed an end-to-end lip sync framework based on audio conditioned latent diffusion model without any intermediate motion representation. (2) To solve the convergence issue of SyncNet, we conducted empirical studies in the aspects of model architecture, training hyperparameters, data preprocessing methods and identified the key factors affecting SyncNet convergence. (3) We proposed the TREPA to improve temporal consistency while preserving the lip-sync accuracy.

## 2. Related Work

### 2.1. Diffusion-based Lip Sync

[34] and [2] are both end-to-end lip sync methods based

on pixel space audio conditioned diffusion models. [57] uses diffusion models in the first stage to complete audio-to-motion conversion and uses a VAE [26] in the second stage for motion-to-image generation. [64] uses transformers in the first stage to convert audio to motion and employs diffusion models in the second stage for motion-to-image generation. [29] uses diffusion autoencoders [37] to convert the masked images into semantic latent codes in the first stage, and uses diffusion models to generate an image conditioned on the semantic latent codes and audio in the second stage, which also belongs to pixel space diffusion models.

### 2.2. Non-diffusion-based Lip Sync

Wav2Lip [36] is the most classic lip sync method that introduced using a pretrained SyncNet [9] to supervise the training of the generator. [20] trains a VQ-VAE [12] to encode faces and head poses, and then trains the lip sync generator in the quantized space to generate high-resolution images. StyleSync [18] follows the overall framework of Wav2Lip, with its main innovation being the use of StyleGAN2 [25] as the generator backbone. [8] divides lip sync into three components: semantic-guided reenactment network, lip sync network, and identity-aware refinement and enhancement. DInet [63] deforms the feature maps to generate mouth shapes conditioned on the driving audio. MuseTalk [61] uses the architecture of Stable Diffusion [41] for inpainting, but it does not perform diffusion process and uses a discriminator for adversarial learning [17], making it more like a GAN-based framework.

## 3. Method

### 3.1. LatentSync Framework

The overview of the LatentSync framework is shown in Fig. 2. Our backbone network generates the video frame by frame without temporal modeling between frames. The temporal consistency during the generation process relies entirely on the audio window. This frame-by-frame generation approach is beneficial for occlusion strategies in dubbing scenarios, as we can easily skip frames where the mouth is occluded and lip sync is not needed. Our framework is based on image-to-image inpainting [43], so it requires a masked image as input. Additionally, to integrate the visual features of the face from the original video, we need to input reference images. The reference images are randomly selected during training to avoid learning shortcuts [16], and they are taken from the current frames during inference. We concatenate these inputs along the channel dimension, so the total input consists of 13 channels (4 channels for noise latent, 1 channel for the mask, 4 channels for the masked image, and 4 channels for the reference image). At the beginning of training, we initialized our model with the parameters of SD 1.5 [41], except for the

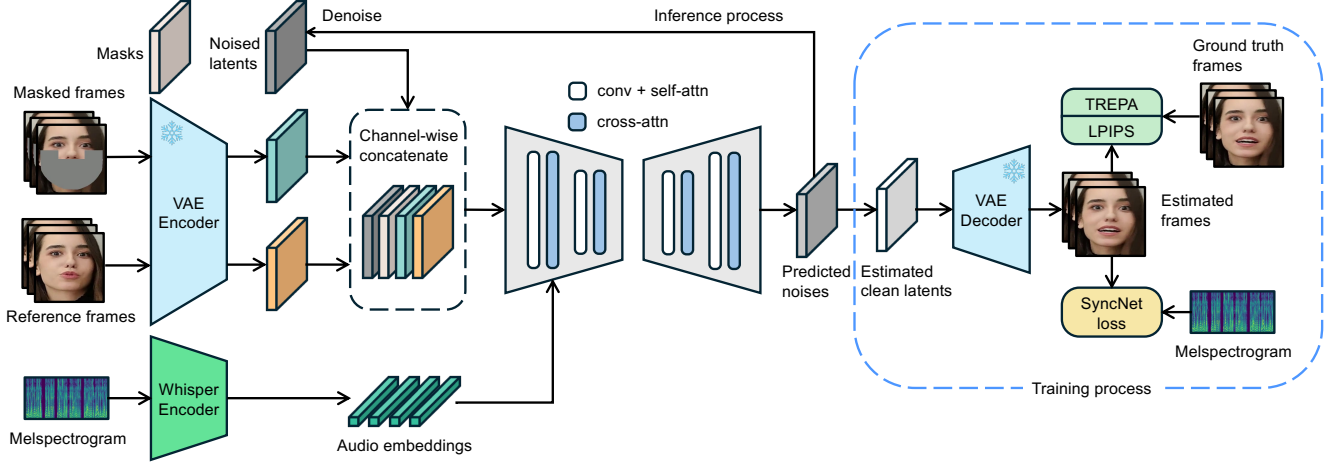


Figure 2. The overview of our LatentSync framework. We use the Whisper [39] to convert melspectrogram into audio embeddings, which are then integrated into the U-Net [42] via cross-attention layers. The reference and masked frames are channel-wise concatenated with noised latents as the input of U-Net. In the training process, we use one-step method to get estimated clean latents from predicted noises, which are then decoded to obtain the estimated clean frames. The TREPA, LPIPS [59] and SyncNet loss [36] are added in the pixel space.

first `conv_in` layer with 13 channels and cross-attention layers of dimension 384, which are randomly initialized. Theoretically, our framework is compatible with more advanced latent diffusion models such as SDXL [35], SD3 [13], and FLUX [28], but we only conducted experiments on SD 1.5 due to hardware limitations.

**Audio layers.** We used the pretrained audio feature extractor Whisper [39] to extract audio embeddings. Lip motion may be influenced by the audio from the surrounding frames, and a larger range of audio input also provides more temporal information for the model. Therefore, for each generated frame, we bundled the audio from several surrounding frames as input. We define the input audio feature  $A^{(f)}$  for the  $f$ th frame as:  $A^{(f)} = \{a^{(f-m)}, \dots, a^{(f)}, \dots, a^{(f+m)}\}$ , where  $m$  is the number of surrounding audio features from one side. To integrate the audio embeddings into the U-Net [42], we used the native cross-attention layer.

**SyncNet supervision.** Our model predicts in the noise space, while SyncNet [9, 36] requires an input in the image space. To address this issue, we use the predicted noise  $\epsilon_\theta(z_t)$  to obtain the estimated  $\hat{z}_0$  in one step, which can be formulated as:

$$\hat{z}_0 = (z_t - \sqrt{1 - \bar{\alpha}_t} \epsilon_\theta(z_t)) / \sqrt{\bar{\alpha}_t} \quad (1)$$

Another problem is that our model makes predictions in the latent space. We explored two methods to add SyncNet supervision to latent diffusion models: (a) **Decoded pixel space supervision**, which trains SyncNet in the same way as [36]. (b) **Latent space supervision**, which requires training a SyncNet in the latent space. The visual encoder input of this SyncNet is the latent vectors obtained by the VAE [12, 26] encoding. The illustration is shown in Fig. 3. We

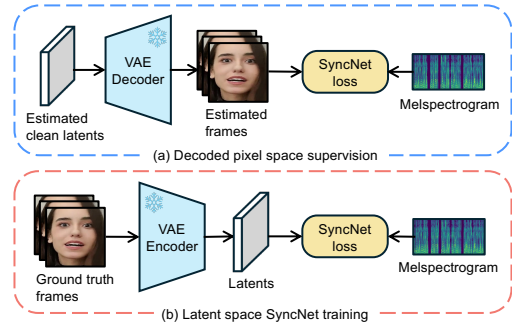


Figure 3. Two methods to add SyncNet supervision to latent diffusion models.

found that training SyncNet in the latent space converges worse compared to training it in the pixel space. We speculate that this is due to information loss in the lip area during the VAE encoding process. The poorer convergence of the latent space SyncNet also results in the worse audio-lip sync accuracy for the supervised diffusion models, according to the experimental results in Sec. 4.3. Therefore, we use decoded pixel space supervision in the LatentSync framework.

**Two-stage training.** In the first stage, we do not decode to the pixel space and do not add SyncNet loss. The purpose of the first stage is to allow the U-Net to learn visual features using a large batch size. Therefore, the training objective of the first stage has only a simple loss [23]:

$$\mathcal{L}_{\text{simple}} = \mathbb{E}_{x, A, \epsilon \sim \mathcal{N}(0,1), t} \left[ \|\epsilon - \epsilon_\theta(z_t, t, \tau_\theta(A))\|_2^2 \right] \quad (2)$$

where  $A$  is the input audio,  $\epsilon_\theta(z_t, t, \tau_\theta(A))$  is the predicted noise, and  $\tau_\theta$  is the audio feature extractor.

In the second stage of training, we used the decoded pixel space supervision method to add SyncNet loss. Com-

pared to [36], we increased the input frame length of SyncNet to 16. For detailed changes to the SyncNet structure, please refer to Sec. 3.3. By using the 16 decoded video frames  $\mathcal{D}(\hat{z}_0)_{f:f+16}$  and the corresponding audio sequence  $a_{f:f+16}$ , the SyncNet loss can be formulated as:

$$\mathcal{L}_{\text{sync}} = \mathbb{E}_{x,a,\epsilon,t} [\text{SyncNet}(\mathcal{D}(\hat{z}_0)_{f:f+16}, a_{f:f+16})] \quad (3)$$

where  $\mathcal{D}$  represents the VAE decoder, since the lipsync task requires generating detailed areas, such as lips, teeth, and facial hair, we used the LPIPS [59] to improve the visual quality of the images generated by the U-Net.

$$\mathcal{L}_{\text{lipps}} = \mathbb{E}_{x,\epsilon,t} \left[ \|\mathcal{V}_l(\mathcal{D}(\hat{z}_0)_f) - \mathcal{V}_l(x_f)\|_2^2 \right] \quad (4)$$

where  $\mathcal{V}_l(\cdot)$  denotes the features extracted from the  $l^{\text{th}}$  layer of a pretrained VGG network [45]. In addition, to improve temporal consistency, we also employed the proposed TREPA, see Eq. (7). For more details of the TREPA, please refer to Sec. 3.2.

The total loss function for the second stage of training is:

$$\mathcal{L}_{\text{total}} = \lambda_1 \mathcal{L}_{\text{simple}} + \lambda_2 \mathcal{L}_{\text{sync}} + \lambda_3 \mathcal{L}_{\text{lipps}} + \lambda_4 \mathcal{L}_{\text{trepa}} \quad (5)$$

We identified the optimal coefficients through empirical analysis as follows:  $(\lambda_1, \lambda_2, \lambda_3, \lambda_4) = (1, 0.05, 0.1, 10)$

**Mixed noise model.** To ensure that the model correctly learns temporal information, the input noises also need to have temporal consistency; otherwise the model will fail to learn properly. The simplest method is applying the same noise to all frames [34]. We further found that diffusion models trained with the mixed noise model [14] exhibit better temporal consistency. The method generates two distinct noise vectors,  $\epsilon_{\text{shared}}$  and  $\epsilon_{\text{ind}}$ .  $\epsilon_{\text{shared}}$  represents a common noise vector applied across all 16 video frames, whereas  $\epsilon_{\text{ind}}$  corresponds to the frame-specific noise. The final noise is obtained through a linear combination of these two vectors.

$$\epsilon^f = \epsilon_{\text{shared}} + \epsilon_{\text{ind}}^f \quad (6)$$

We used the mixed noise model in both two training stages, and we applied the same initial latent noise to all frames in the video during inference stage.

**Affine transformation.** During the data preprocessing stage, affine transformation was employed to achieve face frontalization. This approach [18] helps the model to effectively learn facial features particularly in challenging scenarios such as side-profile views. We applied a mask that covers the entire face to prevent information leakage, ensuring that the model does not infer lip movements based on facial movements. The position and shape of the mask are fixed. We do not use detected landmarks [5, 30] to draw the mask as they will leak information about facial movements. The affine transformation and fixed mask are illustrated in Fig. 4.



Figure 4. The illustration of affine transformation and fixed mask.

### 3.2. Temporal Representation Alignment

TREPA aligns the temporal representations of the generated image sequences with those of ground truth image sequences. The insight behind this method is that merely employing distance loss between individual images only improves the content quality of single generated images but does not enhance the temporal consistency of the generated image sequence. In contrast, temporal representations capture temporal correlation within image sequences, enabling the model to focus on improving the overall temporal consistency. We employed a large-scale self-supervised video model VideoMAE-v2 [52] to extract temporal representations. Due to its unsupervised training on large-scale unlabeled datasets, the model’s temporal representations exhibit strong generalization capabilities, robustness, and high information density.

In mathematical form, let  $\mathcal{T}$  be the self-supervised video model encoder. The encoder’s output is the embedding before the head projection. TREPA can be represented as:

$$\mathcal{L}_{\text{trepa}} = \mathbb{E}_{x,\epsilon,t} \left[ \|\mathcal{T}(\mathcal{D}(\hat{z}_0)_{f:f+16}) - \mathcal{T}(x_{f:f+16})\|_2^2 \right] \quad (7)$$

where the straightforward Mean Squared Error (MSE) is employed to measure the distance between temporal representations. We also fix the representation by  $\ell_2$  normalization before calculating the MSE.

**Observations.** The temporal layer [4, 19] adds temporal self-attention layers to the U-Net to enhance temporal consistency. We initially attempted to apply the temporal layer to LatentSync, but found that it significantly compromised lip-sync accuracy. In contrast, our TREPA not only avoids harming lip-sync accuracy but even improves it to some extent. We hypothesize this is because the temporal layer adds additional parameters to the U-Net, causing some of the gradients in backpropagation to be distributed to the temporal layer parameters, weakening the learning of the audio cross-attention layer parameters. On the other hand, TREPA does not add extra parameters; to improve temporal consistency, the model must rely more effectively on the information in the audio window (since we know that lip-sync models use the audio window to capture temporal information). As a result, the audio cross-attention layers are further trained and strengthened. Refer to the quantitative results in Sec. 4.3.

Another interesting finding is that TREPA can also be applied to improve the temporal consistency and lip-sync accuracy of Wav2Lip [36], according to the experimental re-

sults in Sec. 4.3. Theoretically, any video generation model that generates multiple consecutive frames at once can utilize TREPA to enhance the temporal consistency.

### 3.3. Empirical Studies on SyncNet Convergence

Many researchers have reported the convergence problem of SyncNet on GitHub issues [32, 33, 40, 56], a typical characteristic of this issue is that the training loss gets stuck at 0.69 and fails to decrease further. However, no academic work has provided a detailed analysis of this problem to date. In this section, we analyze the SyncNet convergence problem and identify several critical factors affecting the convergence of SyncNet through various ablation studies. Importantly, we preserved SyncNet’s original training framework and employed the same contrastive loss function as the original paper [9]. Therefore, our experience can be applied to many lip sync [18, 34, 36] and audio-driven portrait animation methods [31] that utilize SyncNet.

**Why is the SyncNet training loss stuck at 0.69?** According to the classic framework of SyncNet [9, 36], we randomly provide SyncNet with positive and negative samples with a 50% probability during the training stage. The output of SyncNet is a probability distribution of whether the sample is positive or negative. We define  $p(x = 1)$  as the probability that the sample is positive, and  $p(x = 0)$  as the probability that the sample is negative. Let  $p(x)$  be the true probability distribution and  $q(x)$  the predicted probability distribution. When  $q(x = 1) \approx q(x = 0) \approx 0.5$  and batch size  $N$  is sufficiently large, the training loss of SyncNet is (proof in Appendix B):

$$\mathcal{L}_{\text{syncnet}} = -\frac{1}{N} \sum_{i=1}^N \sum_{x_i \in \{0,1\}} p(x_i) \log q(x_i) \approx 0.693 \quad (8)$$

This means that SyncNet has not learned any discriminative capability; it is just randomly guessing whether the samples are positive or negative. This may be due to various reasons, including the model’s insufficient capacity to fit the data, the large audio-visual offset in the data, and flaws in the training strategy. In the following paragraphs, we will identify the key factors affecting the convergence of SyncNet through comprehensive ablation studies.

**Batch size.** As shown in Fig. 5, a larger batch size (e.g., 1024) not only enables the model to converge faster and more stably but also results in a lower validation loss at the end of training. In contrast, smaller batch sizes (e.g., 128) may fail to converge, with the loss remaining stuck at 0.69. Even with a slightly larger batch size (e.g., 256), while convergence may be achieved, the training loss exhibits significant oscillations during its descent.

**Architecture.** We attempted to replace the SyncNet’s visual and audio encoders with the U-Net encoder from SD

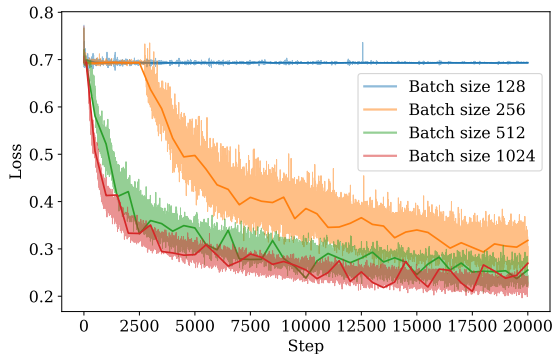


Figure 5. SyncNet training curves of different batch sizes. VoxCeleb2 results, the more transparent curves represent the training set loss, while the darker curves represent the validation set loss; the same applies to the following figures. (VoxCeleb2, Dim 2048, SD residual blocks, 16 frames.)

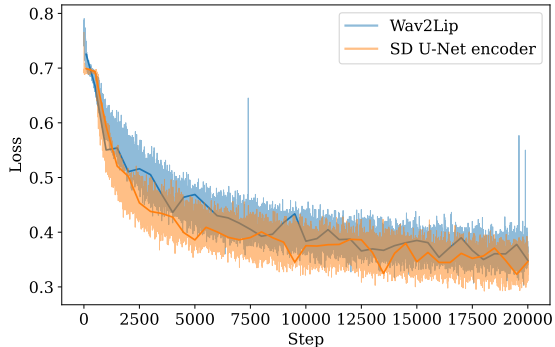


Figure 6. SyncNet training curves of different architectures. For comparison, we also modified the architecture of Wav2Lip’s SyncNet to accept  $256 \times 256$  visual input according to [38]. (VoxCeleb2, Dim 2048, Batch size 512, 5 frames.)

1.5 [41], retaining the structure of residual blocks [21] and self-attention blocks [51] in the U-Net encoder blocks. We only adjusted the downsampling factors based on the size of the input visual images and mel-spectrograms, and we removed the cross-attention blocks, as SyncNet does not require additional conditions. As shown in Fig. 6, SyncNet using the SD U-Net encoder architecture maintained both training loss and validation loss lower than those of Wav2Lip’s SyncNet [36] throughout the training process, though the difference was not substantial.

**Self attention.** We attempted to remove the self-attention [51] blocks in the U-Net encoder, keeping only the residual blocks [21]. As shown in Fig. 7, removing the self-attention blocks results in faster convergence during the initial training phase, while achieving lower validation loss towards the end of the training. Additionally, this approach helps to reduce the model size and accelerates both inference and training speeds. We hypothesize that the reason may be

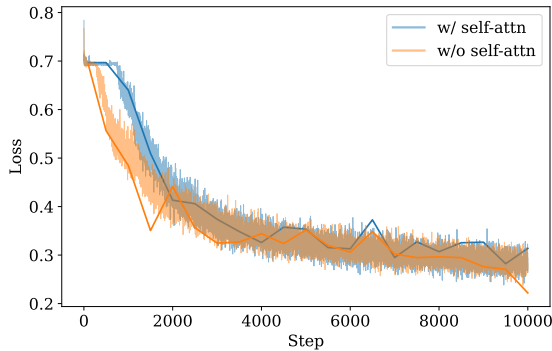


Figure 7. SyncNet training curves with and without self-attention layers. (VoxCeleb2, Dim 2048, Batch size 512, 16 frames.)

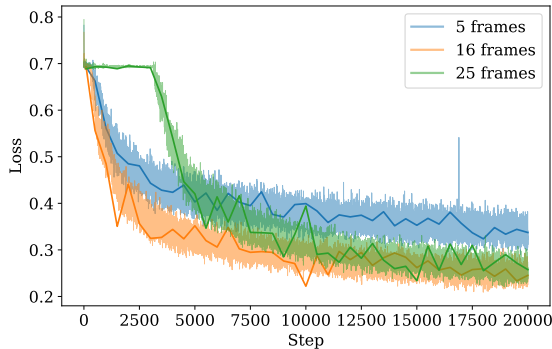


Figure 8. SyncNet training curves of different numbers of input frames. (VoxCeleb2, Batch size 512, SD residual blocks, Dim 2048.)

that attention layers do not possess the inherent inductive biases of CNNs, such as translation equivariance and locality. Therefore, they do not generalize well without sufficient data. Similar findings and explanations can be found in [11].

**Number of frames.** The number of input frames determines the range of visual and audio information that SyncNet can perceive. As shown in Fig. 8, selecting a larger number of frames (e.g., 16) can help the model converge. However, an excessively large number of frames (e.g., 25) will cause the model to get stuck around 0.69 in the early stage of training, and the validation loss at the end of training does not show a significant advantage compared to using 16 frames.

**Data preprocessing.** In-the-wild videos naturally contain audio-visual offsets, so it is necessary to adjust this offset to zero before inputting them into the SyncNet network. We used the official open-source version of SyncNet [9] to adjust the offset and remove videos with  $\text{Sync}_{\text{conf}}$  below 3. Specifically, we tested adjusting the offset before and after applying affine transformation. As shown in Fig. 9, without

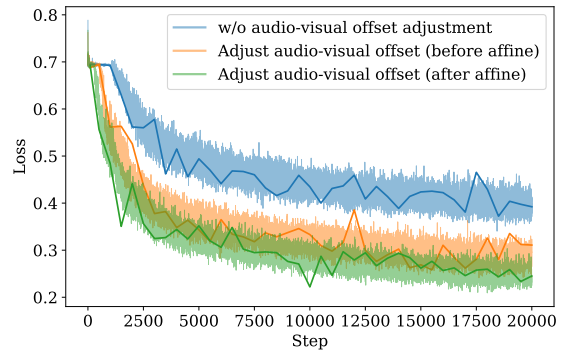


Figure 9. SyncNet training curves of different data preprocessing methods. (VoxCeleb2, Batch size 512, SD residual blocks, Dim 2048, 16 frames.)

offset adjustment, the model’s convergence is significantly impaired. Performing affine transformation before offset adjustment yields better results. We hypothesize that this may be due to affine transformation reducing data with side profiles or unusual angles, allowing the official SyncNet [9] to predict the offset more accurately.

**Discussions.** Based on the ablation studies above, we found that batch size, number of input frames, and data preprocessing method significantly impact SyncNet convergence. The model architecture can also affect convergence, though less noticeably. We identified the optimal settings for a SyncNet with the  $256 \times 256$  input size: batch size of 1024, 16 frames, SD residual blocks for both visual and audio encoders, embedding dimension of 2048, and adjusting the audio-visual offset after affine transformation. We train a SyncNet on VoxCeleb2 [10] and test it on HDTF [62], which is an out-of-distribution experimental setup. The validation loss on VoxCeleb2 reaches around 0.18 and the accuracy on HDTF achieves 94%, which significantly surpasses the previous SOTA result 91% [20, 36]. For more ablation studies, please refer to Appendix C.

## 4. Experiments

### 4.1. Experimental Settings

**Datasets.** We used a mixture of VoxCeleb2 [10] and HDTF [62] datasets as our training set. VoxCeleb2 is a large-scale audio-visual dataset containing over 1 million utterances from over 6,000 speakers. It includes speakers from a wide range of ethnicities, accents, and backgrounds. HDTF contains 362 different high-definition (HD) videos, with resolutions typically around 720p to 1080p.

We used HyperIQA [48] to filter out videos with low visual quality, specifically blurry or pixelated videos. During evaluation, we randomly selected 30 videos from the test set of HDTF or VoxCeleb2.

Method	HDTF				VoxCeleb2			
	FID ↓	SSIM ↑	Sync <sub>conf</sub> ↑	FVD ↓	FID ↓	SSIM ↑	Sync <sub>conf</sub> ↑	FVD ↓
Wav2Lip [36]	12.5	0.70	8.2	304.35	10.8	0.71	7.0	257.85
VideoReTalking [8]	9.5	0.75	7.5	270.56	7.5	0.77	6.4	215.67
DINet [63]	8.02	0.79	7.7	208.93	6.3	0.80	6.7	<b>110.75</b>
MuseTalk [61]	9.35	0.74	6.8	246.75	7.1	0.80	5.9	203.43
LatentSync (Ours)	<b>7.03</b>	<b>0.79</b>	<b>8.9</b>	<b>192.74</b>	<b>5.6</b>	<b>0.81</b>	<b>7.3</b>	124.38

Table 1. Quantitative comparisons on HDTF and VoxCeleb2.

**Implementation details.** When evaluating our model LatentSync, we first converted the videos to 25 FPS, then applied the affine transformation based on facial landmarks detected by face-alignment [5] to obtain  $256 \times 256$  face videos. The audio was resampled to 16kHz. We used 20 steps of DDIM [46] sampling for inference.

**Evaluation metrics.** We evaluate our method in three aspects: (1) Visual quality. We use SSIM [53] in the reconstruction setting and FID [22] in the cross generation setting to assess visual quality. Following [34], the reconstruction setting refers to using the same audio as the input video, while the cross generation setting refers to using audio different from the input video. (2) Lip-sync accuracy. We use the confidence score of SyncNet (Sync<sub>conf</sub>) [9], which we found to align closely with visual assessments. (3) Temporal consistency. We adopt the widely used FVD metric [50].

## 4.2. Comparisons

**Comparison methods.** We selected several SOTA methods that provide open-source inference code and checkpoints for comparison. Wav2Lip [36] is the classic lip-sync method, introducing the idea of using a pretrained SyncNet for supervision instead of a lip-sync discriminator [27]. VideoReTalking [8] divides the lip-sync process into three steps to improve the results. DINet [63] proposed performing deformations on feature maps to achieve high-quality lip sync. MuseTalk [61] utilizes the architecture of Stable Diffusion for inpainting, but it is not based on the diffusion model framework and appears more like a GAN-based approach.

**Quantitative comparisons.** As shown in Tab. 1, the lip-sync accuracy of our method significantly surpasses that of other methods. We believe this may be attributed to our 94% accuracy SyncNet, as well as the audio cross-attention layers, which may better capture the relationship between audio and lip movements. In terms of visual quality, our method outperforms others, likely due to the capabilities of the Stable Diffusion model. Owing to the incorporation of TREPA, our FVD score is also superior to other methods.

**Qualitative comparisons.** We run two cases in the cross

Method	Sync <sub>conf</sub> ↑	FVD ↓
LatentSync w/o SyncNet	1.6	260.37
LatentSync + latent space SyncNet	7.9	240.45
LatentSync + pixel space SyncNet	<b>8.9</b>	<b>192.74</b>

Table 2. The ablation studies of different SyncNets. HDTF results.

generation setting. According to Fig. 10, Wav2Lip has excellent lip-sync accuracy, but the generated videos are very blurry. VideoReTalking shows strange artifacts. DINet’s generated box is obvious, and its mouth movements are stiff. MuseTalk does not preserve facial features well, the man’s beard becomes sparse. In contrast, our method excels in both clarity and identity preservation, even the mole on the woman’s face was preserved. Furthermore, it hardly shows generated box due to the smooth shape of fixed mask.

## 4.3. Ablation studies

**The supervision effect of SyncNet.** As shown in Tab. 2, when the SyncNet supervision is not added, the trained diffusion models have no lipsync ability at all. In fact, we found that other end-to-end lipsync methods [34, 36] exhibit similar phenomena. As for supervision in two different spaces, diffusion models under pixel space SyncNet supervision perform better in terms of lip-sync accuracy and temporal consistency. This is likely due to the poor convergence of latent space SyncNet supervision (as shown in Fig. 11), which is quite reasonable since the input to the latent space SyncNet is the compressed latents obtained from VAE encoding, and some lip information may already be lost.

In addition, we found that improvements in lip-sync accuracy were accompanied by an increase in temporal consistency. This is because the temporal consistency of our model is provided by the audio window; as the model becomes better at utilizing audio information, temporal consistency also improves accordingly.

**Different methods for improving temporal consistency.** According to Tab. 3, the temporal layer significantly improves temporal consistency but also noticeably harms lip-sync accuracy. Our TREPA achieves balanced improvements in both lip-sync accuracy and temporal consistency

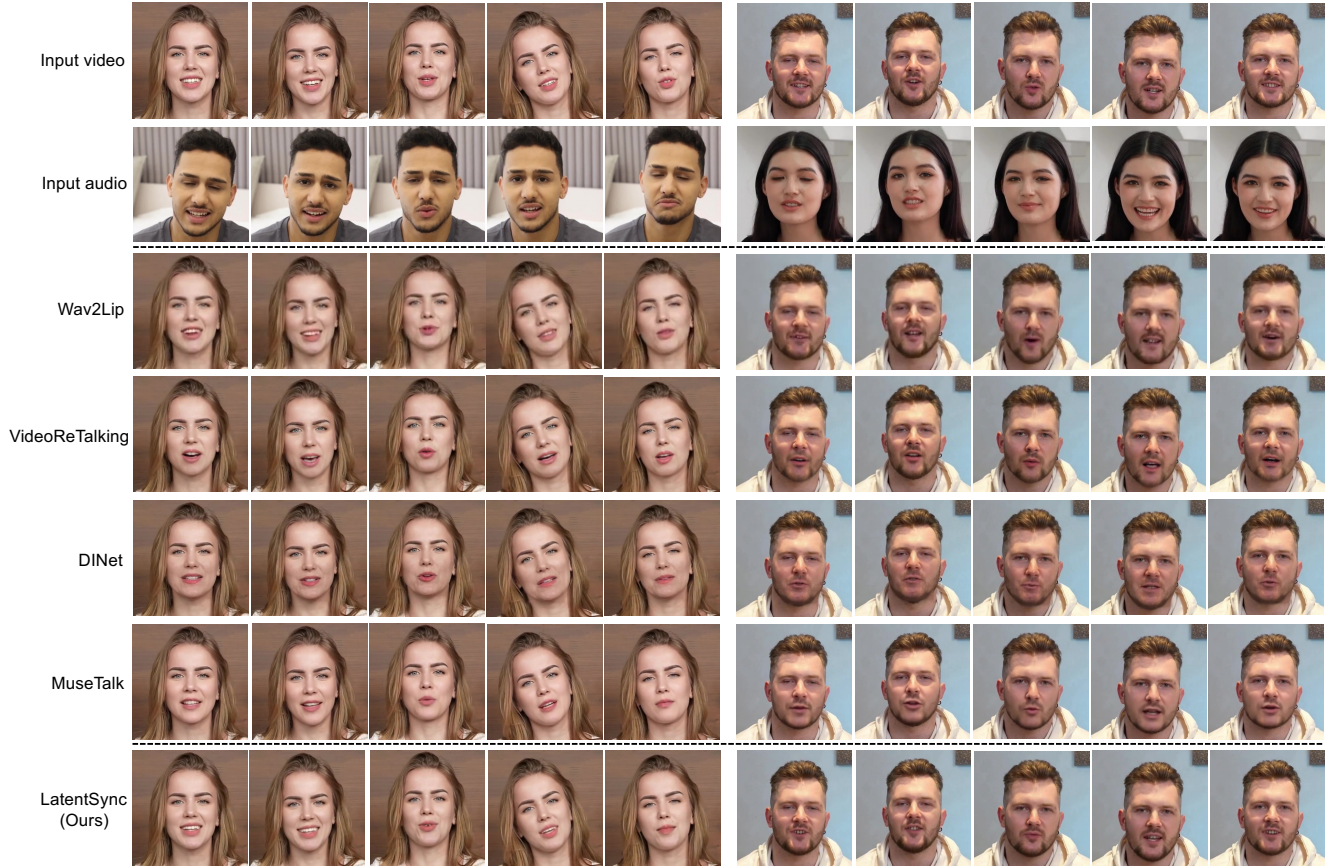


Figure 10. Qualitative comparisons with SOTA lip-sync methods. We run two cases in the cross generation setting [34]. The first row demonstrates the original input video, and the second row is the video from which we extracted the audio as input, the video can be regarded as the target lip movements. Rows 3 ~ 7 display the lip-synced videos. (All the photorealistic portrait images in this paper are from licensed models.)

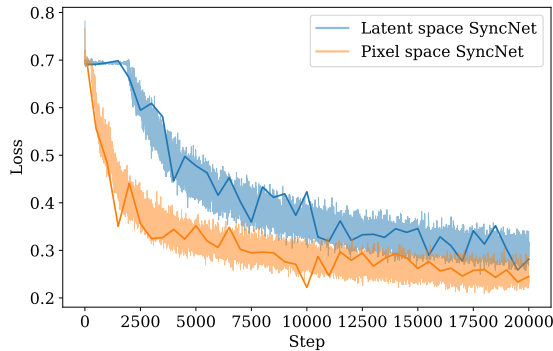


Figure 11. SyncNet training curves of different visual input spaces. Here we use the open-sourced pretrained VAE from Stability AI [1] for encoding. (VoxCeleb2, Batch size 512, SD residual blocks, Dim 1024, 16 frames.)

without evident drawbacks. Considering the importance of lip-sync accuracy, TREPA is obviously the better approach.

In addition, TREPA can also improve Wav2Lip accord-

Method	Sync <sub>conf</sub> ↑	FVD ↓
LatentSync	8.2	234.35
LatentSync + Temporal layer [19]	4.7	<b>174.56</b>
LatentSync + TREPA	<b>8.9</b>	192.74

Table 3. The ablation studies of different methods for improving temporal consistency. HDTF results.

Method	Sync <sub>conf</sub> ↑	FVD ↓
Wav2Lip	8.2	304.35
Wav2Lip + TREPA	<b>8.6</b>	<b>264.56</b>

Table 4. The ablation studies of Wav2Lip with TREPA. HDTF results.

ing to Tab. 4, which suggests that our method has general applicability in lip-sync tasks.

## 5. Conclusion

We introduced a new lip sync framework named LatentSync that addresses the problems of traditional diffusion-based



lip sync methods: (1) The low sampling speed and inability to generate high-resolution videos of pixel space diffusion. (2) The information loss in two-stage generation methods. In addition, we proposed TREPA to improve temporal consistency while preserving the lip-sync accuracy, which mitigates the problem of video flickering in diffusion-based lip sync methods. Furthermore, we analyzed the notorious SyncNet convergence issue and conducted comprehensive ablation studies to identify several key influencing factors.

## References

- [1] Stability AI. sd-vae-ft-mse. <https://huggingface.co/stabilityai/sd-vae-ft-mse>, 2022. 8
- [2] Dan Bigioi, Shubhajit Basak, Michał Stypułkowski, Maciej Zieba, Hugh Jordan, Rachel McDonnell, and Peter Corcoran. Speech driven video editing via an audio-conditioned diffusion model. *Image and Vision Computing*, 142:104911, 2024. 1, 2
- [3] Volker Blanz and Thomas Vetter. A morphable model for the synthesis of 3d faces. In *Seminal Graphics Papers: Pushing the Boundaries, Volume 2*, pages 157–164. 2023. 2
- [4] Andreas Blattmann, Robin Rombach, Huan Ling, Tim Dockhorn, Seung Wook Kim, Sanja Fidler, and Karsten Kreis. Align your latents: High-resolution video synthesis with latent diffusion models. In *Proceedings of the IEEE/CVF Conference on Computer Vision and Pattern Recognition*, pages 22563–22575, 2023. 4
- [5] Adrian Bulat and Georgios Tzimiropoulos. How far are we from solving the 2d & 3d face alignment problem?(and a dataset of 230,000 3d facial landmarks). In *Proceedings of the IEEE international conference on computer vision*, pages 1021–1030, 2017. 2, 4, 7
- [6] Tong Che, Yanran Li, Athul Paul Jacob, Yoshua Bengio, and Wenjie Li. Mode regularized generative adversarial networks. *arXiv preprint arXiv:1612.02136*, 2016. 1
- [7] Zhiyuan Chen, Jiajiong Cao, Zhiquan Chen, Yuming Li, and Chenguang Ma. Echomimic: Lifelike audio-driven portrait animations through editable landmark conditions. *arXiv preprint arXiv:2407.08136*, 2024. 1
- [8] Kun Cheng, Xiaodong Cun, Yong Zhang, Menghan Xia, Fei Yin, Mingrui Zhu, Xuan Wang, Jue Wang, and Nannan Wang. Videoretalking: Audio-based lip synchronization for talking head video editing in the wild. In *SIGGRAPH Asia 2022 Conference Papers*, pages 1–9, 2022. 2, 7
- [9] Joon Son Chung and Andrew Zisserman. Out of time: automated lip sync in the wild. In *Computer Vision—ACCV 2016 Workshops: ACCV 2016 International Workshops, Taipei, Taiwan, November 20–24, 2016, Revised Selected Papers, Part II 13*, pages 251–263. Springer, 2017. 2, 3, 5, 6, 7, 1
- [10] Joon Son Chung, Arsha Nagrani, and Andrew Zisserman. Voxceleb2: Deep speaker recognition. *arXiv preprint arXiv:1806.05622*, 2018. 6, 1
- [11] Alexey Dosovitskiy. An image is worth 16x16 words: Transformers for image recognition at scale. *arXiv preprint arXiv:2010.11929*, 2020. 6
- [12] Patrick Esser, Robin Rombach, and Bjorn Ommer. Taming transformers for high-resolution image synthesis. In *Proceedings of the IEEE/CVF conference on computer vision and pattern recognition*, pages 12873–12883, 2021. 2, 3
- [13] Patrick Esser, Sumith Kulal, Andreas Blattmann, Rahim Entezari, Jonas Müller, Harry Saini, Yam Levi, Dominik Lorenz, Axel Sauer, Frederic Boesel, et al. Scaling rectified flow transformers for high-resolution image synthesis. In *Forty-first International Conference on Machine Learning*, 2024. 3
- [14] Songwei Ge, Seungjun Nah, Guilin Liu, Tyler Poon, Andrew Tao, Bryan Catanzaro, David Jacobs, Jia-Bin Huang, Ming-Yu Liu, and Yogesh Balaji. Preserve your own correlation: A noise prior for video diffusion models. In *Proceedings of the IEEE/CVF International Conference on Computer Vision*, pages 22930–22941, 2023. 4
- [15] Songwei Ge, Aniruddha Mahapatra, Gaurav Parmar, Jun-Yan Zhu, and Jia-Bin Huang. On the content bias in fréchet video distance. In *Proceedings of the IEEE/CVF Conference on Computer Vision and Pattern Recognition*, pages 7277–7288, 2024. 2
- [16] Robert Geirhos, Jörn-Henrik Jacobsen, Claudio Michaelis, Richard Zemel, Wieland Brendel, Matthias Bethge, and Felix A Wichmann. Shortcut learning in deep neural networks. *Nature Machine Intelligence*, 2(11):665–673, 2020. 2
- [17] Ian Goodfellow, Jean Pouget-Abadie, Mehdi Mirza, Bing Xu, David Warde-Farley, Sherjil Ozair, Aaron Courville, and Yoshua Bengio. Generative adversarial nets. *Advances in neural information processing systems*, 27, 2014. 2
- [18] Jiazhi Guan, Zhanwang Zhang, Hang Zhou, Tianshu Hu, Kaisiyuan Wang, Dongliang He, Haocheng Feng, Jingtuo Liu, Errui Ding, Ziwei Liu, et al. Stylesync: High-fidelity generalized and personalized lip sync in style-based generator. In *Proceedings of the IEEE/CVF Conference on Computer Vision and Pattern Recognition*, pages 1505–1515, 2023. 1, 2, 4, 5
- [19] Yuwei Guo, Ceyuan Yang, Anyi Rao, Zhengyang Liang, Yaohui Wang, Yu Qiao, Maneesh Agrawala, Dahua Lin, and Bo Dai. Animatediff: Animate your personalized text-to-image diffusion models without specific tuning. *arXiv preprint arXiv:2307.04725*, 2023. 4, 8
- [20] Ankit Gupta, Rudrabha Mukhopadhyay, Sindhu Balachandra, Faizan Farooq Khan, Vinay P Nambodiri, and CV Jawahar. Towards generating ultra-high resolution talking-face videos with lip synchronization. In *Proceedings of the IEEE/CVF Winter Conference on Applications of Computer Vision*, pages 5209–5218, 2023. 2, 6
- [21] Kaiming He, Xiangyu Zhang, Shaoqing Ren, and Jian Sun. Deep residual learning for image recognition. In *Proceedings of the IEEE conference on computer vision and pattern recognition*, pages 770–778, 2016. 5
- [22] Martin Heusel, Hubert Ramsauer, Thomas Unterthiner, Bernhard Nessler, and Sepp Hochreiter. Gans trained by a two time-scale update rule converge to a local nash equilibrium. *Advances in neural information processing systems*, 30, 2017. 7
- [23] Jonathan Ho, Ajay Jain, and Pieter Abbeel. Denoising diffusion probabilistic models. *Advances in neural information processing systems*, 33:6840–6851, 2020. 3
- [24] Minguk Kang, Jun-Yan Zhu, Richard Zhang, Jaesik Park, Eli Shechtman, Sylvain Paris, and Taesung Park. Scaling up gans for text-to-image synthesis. In *Proceedings of the IEEE/CVF Conference on Computer Vision and Pattern Recognition*, pages 10124–10134, 2023. 1
- [25] Tero Karras, Samuli Laine, Miika Aittala, Janne Hellsten, Jaakko Lehtinen, and Timo Aila. Analyzing and improving the image quality of stylegan. In *Proceedings of*

- the *IEEE/CVF conference on computer vision and pattern recognition*, pages 8110–8119, 2020. 2
- [26] Diederik P Kingma. Auto-encoding variational bayes. *arXiv preprint arXiv:1312.6114*, 2013. 2, 3
- [27] Prajwal KR, Rudrabha Mukhopadhyay, Jerin Philip, Abhishek Jha, Vinay Namboodiri, and CV Jawahar. Towards automatic face-to-face translation. In *Proceedings of the 27th ACM international conference on multimedia*, pages 1428–1436, 2019. 7
- [28] Black Forest Labs. Flux. <https://github.com/black-forest-labs/flux>, 2024. 3
- [29] Tao Liu, Chenpeng Du, Shuai Fan, Feilong Chen, and Kai Yu. Diffdub: Person-generic visual dubbing using inpainting renderer with diffusion auto-encoder. In *ICASSP 2024-2024 IEEE International Conference on Acoustics, Speech and Signal Processing (ICASSP)*, pages 3630–3634. IEEE, 2024. 1, 2
- [30] Camillo Lugaresi, Jiuqiang Tang, Hadon Nash, Chris McClanahan, Esha Ubowaja, Michael Hays, Fan Zhang, Chuoling Chang, Ming Guang Yong, Juhyun Lee, et al. Mediapipe: A framework for building perception pipelines. *arXiv preprint arXiv:1906.08172*, 2019. 2, 4
- [31] Yifeng Ma, Shiwei Zhang, Jiayu Wang, Xiang Wang, Yingya Zhang, and Zhidong Deng. Dreamtalk: When expressive talking head generation meets diffusion probabilistic models. *arXiv preprint arXiv:2312.09767*, 2023. 5, 1
- [32] Mayur. Expert lip-sync discriminator is not converging on lrs2? <https://github.com/Rudrabha/Wav2Lip/issues/298>, 2021. 5
- [33] mrlhellohorld. train lip-sync expert model have not declined on my custom dataset. <https://github.com/Rudrabha/Wav2Lip/issues/419>, 2022. 5
- [34] Soumik Mukhopadhyay, Saksham Suri, Ravi Teja Gadde, and Abhinav Shrivastava. Diff2lip: Audio conditioned diffusion models for lip-synchronization. In *Proceedings of the IEEE/CVF Winter Conference on Applications of Computer Vision*, pages 5292–5302, 2024. 1, 2, 4, 5, 7, 8
- [35] Dustin Podell, Zion English, Kyle Lacey, Andreas Blattmann, Tim Dockhorn, Jonas Müller, Joe Penna, and Robin Rombach. Sdxl: Improving latent diffusion models for high-resolution image synthesis. *arXiv preprint arXiv:2307.01952*, 2023. 3
- [36] KR Prajwal, Rudrabha Mukhopadhyay, Vinay P Namboodiri, and CV Jawahar. A lip sync expert is all you need for speech to lip generation in the wild. In *Proceedings of the 28th ACM international conference on multimedia*, pages 484–492, 2020. 1, 2, 3, 4, 5, 6, 7
- [37] Konpat Preechakul, Nattanat Chatthee, Suttisak Widadwongsa, and Supasorn Suwajanakorn. Diffusion autoencoders: Toward a meaningful and decodable representation. In *Proceedings of the IEEE/CVF conference on computer vision and pattern recognition*, pages 10619–10629, 2022. 2
- [38] primepake. wav2lip 288x288. [https://github.com/primepake/wav2lip\\_288x288](https://github.com/primepake/wav2lip_288x288), 2021. 5
- [39] Alec Radford, Jong Wook Kim, Tao Xu, Greg Brockman, Christine McLeavey, and Ilya Sutskever. Robust speech recognition via large-scale weak supervision. In *International conference on machine learning*, pages 28492–28518. PMLR, 2023. 3
- [40] rizwanishaq. Expert syncnet training? <https://github.com/Rudrabha/Wav2Lip/issues/195>, 2021. 5
- [41] Robin Rombach, Andreas Blattmann, Dominik Lorenz, Patrick Esser, and Björn Ommer. High-resolution image synthesis with latent diffusion models. In *Proceedings of the IEEE/CVF conference on computer vision and pattern recognition*, pages 10684–10695, 2022. 2, 5, 1
- [42] Olaf Ronneberger, Philipp Fischer, and Thomas Brox. U-net: Convolutional networks for biomedical image segmentation. In *Medical image computing and computer-assisted intervention—MICCAI 2015: 18th international conference, Munich, Germany, October 5-9, 2015, proceedings, part III 18*, pages 234–241. Springer, 2015. 3
- [43] Chitwan Saharia, William Chan, Huiwen Chang, Chris Lee, Jonathan Ho, Tim Salimans, David Fleet, and Mohammad Norouzi. Palette: Image-to-image diffusion models. In *ACM SIGGRAPH 2022 conference proceedings*, pages 1–10, 2022. 2
- [44] Axel Sauer, Tero Karras, Samuli Laine, Andreas Geiger, and Timo Aila. Stylegan-t: Unlocking the power of gans for fast large-scale text-to-image synthesis. In *International conference on machine learning*, pages 30105–30118. PMLR, 2023. 1
- [45] Karen Simonyan and Andrew Zisserman. Very deep convolutional networks for large-scale image recognition. *arXiv preprint arXiv:1409.1556*, 2014. 4
- [46] Jiaming Song, Chenlin Meng, and Stefano Ermon. Denoising diffusion implicit models. *arXiv preprint arXiv:2010.02502*, 2020. 7
- [47] Akash Srivastava, Lazar Valkov, Chris Russell, Michael U Gutmann, and Charles Sutton. Veegan: Reducing mode collapse in gans using implicit variational learning. *Advances in neural information processing systems*, 30, 2017. 1
- [48] Shaolin Su, Qingsen Yan, Yu Zhu, Cheng Zhang, Xin Ge, Jinqiu Sun, and Yanning Zhang. Blindly assess image quality in the wild guided by a self-adaptive hyper network. In *Proceedings of the IEEE/CVF conference on computer vision and pattern recognition*, pages 3667–3676, 2020. 6
- [49] Linrui Tian, Qi Wang, Bang Zhang, and Liefeng Bo. Emo: Emote portrait alive-generating expressive portrait videos with audio2video diffusion model under weak conditions. *arXiv preprint arXiv:2402.17485*, 2024. 1
- [50] Thomas Unterthiner, Sjoerd Van Steenkiste, Karol Kurach, Raphael Marinier, Marcin Michalski, and Sylvain Gelly. Towards accurate generative models of video: A new metric & challenges. *arXiv preprint arXiv:1812.01717*, 2018. 7
- [51] A Vaswani. Attention is all you need. *Advances in Neural Information Processing Systems*, 2017. 5
- [52] Limin Wang, Bingkun Huang, Zhiyu Zhao, Zhan Tong, Yinan He, Yi Wang, Yali Wang, and Yu Qiao. Videomae v2: Scaling video masked autoencoders with dual masking. In *Proceedings of the IEEE/CVF Conference on Computer Vision and Pattern Recognition*, pages 14549–14560, 2023. 2, 4

- [53] Zhou Wang, Alan C Bovik, Hamid R Sheikh, and Eero P Simoncelli. Image quality assessment: from error visibility to structural similarity. *IEEE transactions on image processing*, 13(4):600–612, 2004. 7
- [54] Mingwang Xu, Hui Li, Qingkun Su, Hanlin Shang, Liwei Zhang, Ce Liu, Jingdong Wang, Luc Van Gool, Yao Yao, and Siyu Zhu. Hallo: Hierarchical audio-driven visual synthesis for portrait image animation. *arXiv preprint arXiv:2406.08801*, 2024. 1
- [55] Sicheng Xu, Guojun Chen, Yu-Xiao Guo, Jiaolong Yang, Chong Li, Zhenyu Zang, Yizhong Zhang, Xin Tong, and Baining Guo. Vasa-1: Lifelike audio-driven talking faces generated in real time. *arXiv preprint arXiv:2404.10667*, 2024. 1
- [56] yonglianglan. expert syncnet loss remains at 0.69 and does not converge. <https://github.com/Rudrabha/Wav2Lip/issues/296>, 2021. 5
- [57] Runyi Yu, Tianyu He, Ailing Zeng, Yuchi Wang, Junliang Guo, Xu Tan, Chang Liu, Jie Chen, and Jiang Bian. Make your actor talk: Generalizable and high-fidelity lip sync with motion and appearance disentanglement. *arXiv preprint arXiv:2406.08096*, 2024. 1, 2
- [58] Sihyun Yu, Sangkyung Kwak, Huiwon Jang, Jongheon Jeong, Jonathan Huang, Jinwoo Shin, and Saining Xie. Representation alignment for generation: Training diffusion transformers is easier than you think. *arXiv preprint arXiv:2410.06940*, 2024. 2
- [59] Richard Zhang, Phillip Isola, Alexei A Efros, Eli Shechtman, and Oliver Wang. The unreasonable effectiveness of deep features as a perceptual metric. In *Proceedings of the IEEE conference on computer vision and pattern recognition*, pages 586–595, 2018. 2, 3, 4
- [60] Wenxuan Zhang, Xiaodong Cun, Xuan Wang, Yong Zhang, Xi Shen, Yu Guo, Ying Shan, and Fei Wang. Sadtalker: Learning realistic 3d motion coefficients for stylized audio-driven single image talking face animation. In *Proceedings of the IEEE/CVF Conference on Computer Vision and Pattern Recognition*, pages 8652–8661, 2023. 1
- [61] Yue Zhang, Minhao Liu, Zhaokang Chen, Bin Wu, Yubin Zeng, Chao Zhan, Yingjie He, Junxin Huang, and Wenjiang Zhou. Musetalk: Real-time high quality lip synchronization with latent space inpainting. *arXiv preprint arXiv:2410.10122*, 2024. 2, 7, 1
- [62] Zhimeng Zhang, Lincheng Li, Yu Ding, and Changjie Fan. Flow-guided one-shot talking face generation with a high-resolution audio-visual dataset. In *Proceedings of the IEEE/CVF Conference on Computer Vision and Pattern Recognition*, pages 3661–3670, 2021. 2, 6
- [63] Zhimeng Zhang, Zhipeng Hu, Wenjin Deng, Changjie Fan, Tangjie Lv, and Yu Ding. Dinet: Deformation inpainting network for realistic face visually dubbing on high resolution video. In *Proceedings of the AAAI Conference on Artificial Intelligence*, pages 3543–3551, 2023. 2, 7
- [64] Weizhi Zhong, Jichang Li, Yinqi Cai, Liang Lin, and Guanbin Li. Style-preserving lip sync via audio-aware style reference. *arXiv preprint arXiv:2408.05412*, 2024. 1, 2

# Appendix

## A. The Differences between Lip Sync and Audio-driven Portrait Animation

Many people may confuse lip sync with audio-driven portrait animation. These two tasks have some similarities but are actually completely different tasks. Their main difference lies in the input:

- The inputs of Lip Sync: **Video** + Audio
- The inputs of Audio-driven Portrait Animation: **Image** + Audio

This leads to differences in their overall frameworks. Lip sync is more like a video-to-video editing framework, which needs to keep areas other than the mouth the same as in the input video. Audio-driven portrait animation is more like an image-to-video animation framework, which can change the head’s movement and even facial expressions. The differences in the overall frameworks result in substantial differences in their training and inference methods. We list some methods for the two different tasks to help readers better distinguish between them:

- Lip Sync: Wav2Lip[36], Diff2Lip [34], StyleSync [18], MuseTalk [61], MyTalk [57]
- Audio-driven Portrait Animation: EMO [49], Hallo [54], EchoMimic [7], VASA-1 [55], DreamTalk [31], SadTalker [60]

Although there are already some audio-driven portrait animation methods based on Stable Diffusion [41], such as EMO [49] and Hallo [54], it is hard to adapt them for the lip sync task. For example, the temporal layer is very effective in these methods, but we found that it is not suitable for the lip sync task. To the best of our knowledge, the methods closest to ours are Diff2Lip [34] and MyTalk [57], which are pixel space diffusion and two-stage generation methods.

## B. SyncNet Training Loss Proof

According to the classic framework of SyncNet [9, 36], we randomly provide SyncNet with positive and negative samples with a 50% probability during the training stage. The output of SyncNet is a probability distribution of whether the sample is positive or negative. We define  $p(x = 1)$  as the probability that the sample is positive, and  $p(x = 0)$  as the probability that the sample is negative. Let  $p(x)$  be the true probability distribution and  $q(x)$  the predicted probability distribution. We plot some scatter charts to observe the changes in the prediction probabilities of a non-converging SyncNet during the training process.

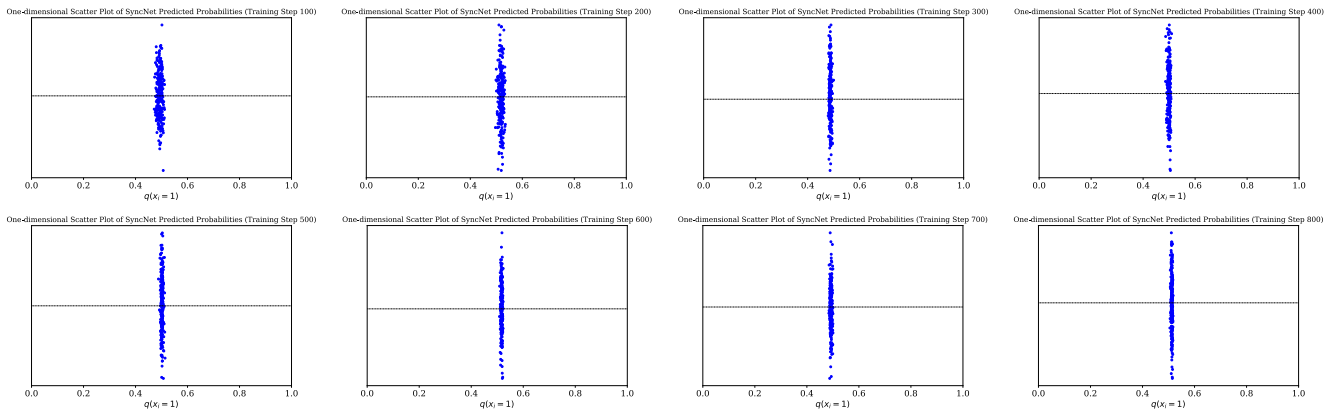


Figure 12. We train a SyncNet on VoxCeleb2 [10] with batch size of 256. We modify its architecture and data to make it non-converging. Every 100 steps, we plot a scatter plot to observe the probability distribution of SyncNet’s predicted  $q(x_i = 1)$ , including 256 data points. The x-axis represents the probability  $q(x_i = 1)$ , and we add some random jitter along the y-axis for better visualization.

As shown in Fig. 12, in the early stages of training, the probabilities predicted by SyncNet for  $q(x_i = 1)$  are dispersed, but later in the training, the probabilities for  $q(x_i = 1)$  are almost all distributed around 0.5 (the scatter charts for  $q(x_i = 0)$  are similar). Now we have:

$$\forall i \in 1, 2, \dots, N : q(x_i = 1) \approx q(x_i = 0) \approx 0.5 \quad (9)$$

We speculate that this may be because, the non-converging SyncNet is consistently unable to correctly distinguish whether a sample is positive or negative during the training process. However, to reduce the training loss, it tends to output a probability

of 0.5 for all input embeddings to minimize the training loss as much as possible. This is why the training loss decreases somewhat initially and then gets stuck (from 0.8 to 0.69).

We assume that there are  $A$  positive samples and  $B$  negative samples in a batch, and then we can derive SyncNet’s training loss based on the following steps:

$$\mathcal{L}_{\text{syncnet}} = -\frac{1}{N} \sum_{i=1}^N \sum_{x_i \in \{0,1\}} p(x_i) \log q(x_i) \quad (10)$$

$$= -\frac{1}{N} \sum_{i=1}^N [p(x_i = 1) \log q(x_i = 1) + p(x_i = 0) \log q(x_i = 0)] \quad (11)$$

$$= -\frac{1}{N} \sum_{i=1}^N p(x_i = 1) \log q(x_i = 1) - \frac{1}{N} \sum_{i=1}^N p(x_i = 0) \log q(x_i = 0) \quad (12)$$

$$= -\frac{1}{N} \left[ \sum_{a=1}^A 1 \times \log q(x_a = 1) + \sum_{b=1}^B 0 \times \log q(x_b = 1) \right] - \frac{1}{N} \left[ \sum_{a=1}^A 0 \times \log q(x_a = 1) + \sum_{b=1}^B 1 \times \log q(x_b = 1) \right] \quad (13)$$

$$= -\frac{1}{N} \left[ \sum_{a=1}^A \log q(x_a = 1) + \sum_{b=1}^B \log q(x_b = 0) \right] \quad (14)$$

$$\approx -\frac{1}{N} [A \log 0.5 + B \log 0.5] \quad \text{Apply Eq. (9)} \quad (15)$$

$$= 0.693 \quad (16)$$

## C. Additional SyncNet Ablation Studies

### C.1. Embedding dimension

The dimensions of the audio and visual embeddings in SyncNet should be carefully calibrated to a moderate size. As illustrated in Fig. 13, embeddings with smaller dimensions (e.g., 512) result in representations that fail to capture sufficient semantic information, while larger dimensions (e.g., 4096 or 6144) lead to sparse representations, thereby impeding model convergence. Through empirical analysis, we identified that an optimal embedding dimension of 2048 is suitable for images with an input resolution of  $256 \times 256$  pixels. For images of varying resolutions, the embedding dimensions should be appropriately scaled to ensure optimal performance.

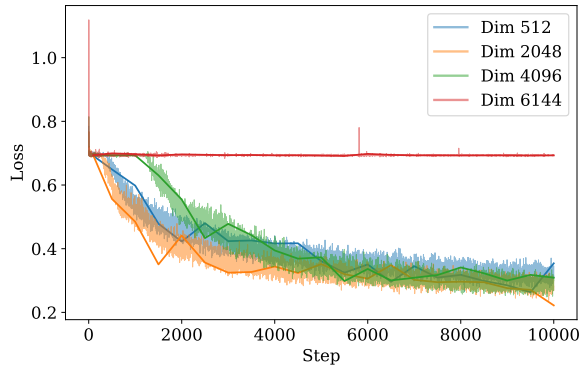


Figure 13. SyncNet training curves of different embedding dimensions. (VoxCeleb2, Batch size 512, SD residual blocks, 16 frames.)